Volume 16
Number 8
27 April 2026
Pages 2553–3002

Catalysis Science & Technology

rsc.li/catalysis

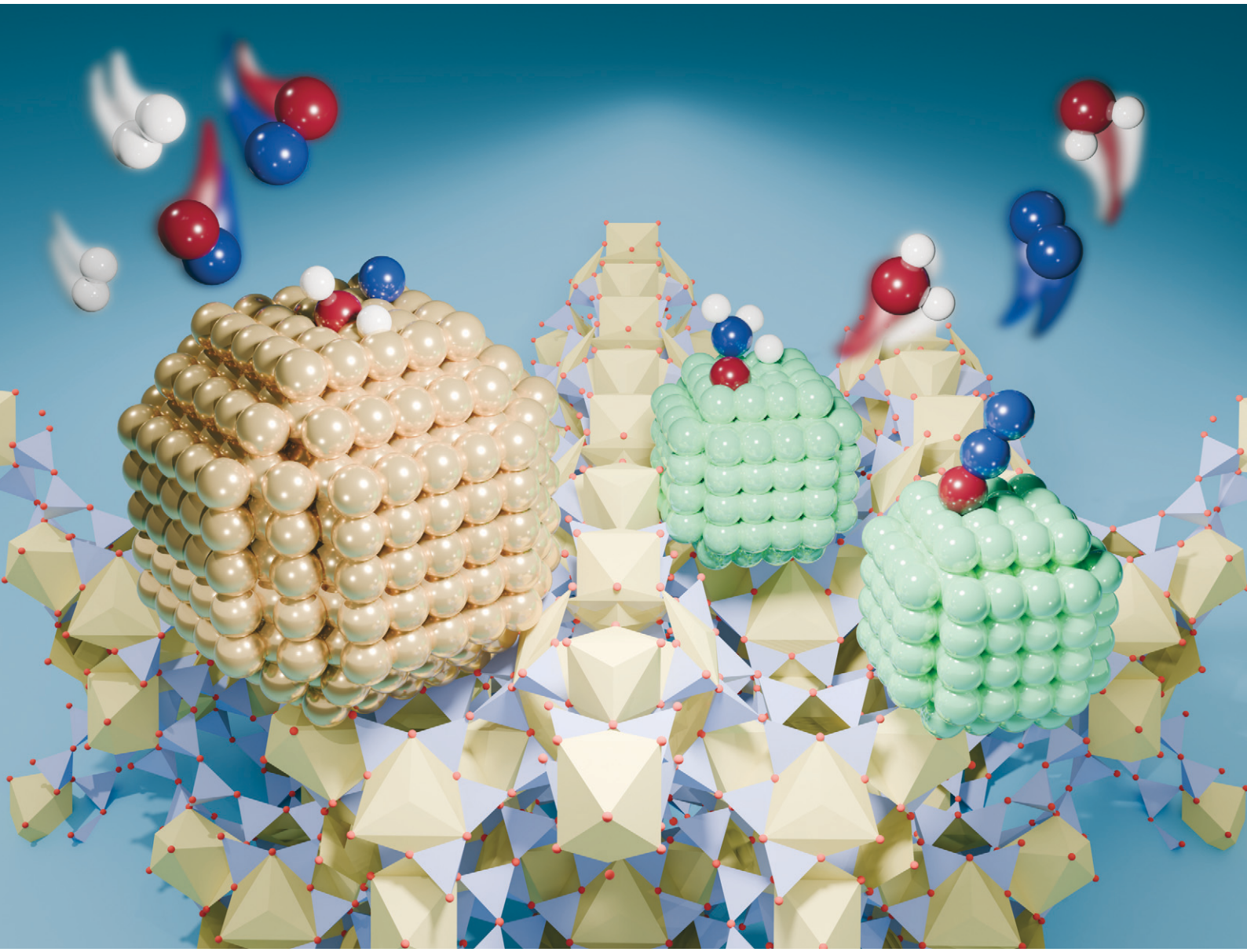

ISSN 2044-4761

ROYAL SOCIETY OF CHEMISTRY

PAPER

Patrick Lott *et al.*

Enhancing the performance of Pd/zeolite-based H_2-SCR catalysts: the role of noble metal loading, promoter addition, and combination with a conventional Fe-BEA NH_3-SCR catalyst

Catalysis Science & Technology

ROYAL SOCIETY OF CHEMISTRY

PAPER

View Article Online
View Journal | View Issue

Cite this: *Catal. Sci. Technol.*, 2026, **16**, 2680

Enhancing the performance of Pd/zeolite-based H_2-SCR catalysts: the role of noble metal loading, promoter addition, and combination with a conventional Fe-BEA NH_3-SCR catalyst

Michael Borchers,† Daniel Hodonj,† Kathrin Schäfer, Frank Manuel Bauer and Patrick Lott *

The direct utilization of hydrogen (H_2) as a reductant in the selective catalytic reduction (SCR) of nitrogen oxides (NO_x) presents a promising strategy for mitigating emissions from hydrogen-fueled internal combustion engines (H_2-ICEs). Despite recent advancements, H_2-SCR suffers from a narrow operational temperature window and limited product selectivity. In this study, Pd/TiO_2/HY catalysts with varying palladium loadings were synthesized, characterized, and evaluated for their catalytic performance. A strong correlation between NO conversion and H_2 activation was observed, particularly at low temperatures, with higher Pd content enhancing pollutant abatement. The incorporation of tungsten oxide (WO_3) as a promoter improved catalytic activity and suppressed ammonia (NH_3) formation under both dry and humid conditions, albeit at the cost of increased nitrous oxide (N_2O) emissions. Alternatively, vanadia (V_2O_5) addition reduced secondary emissions but compromised NO_x conversion efficiency. A bifunctional catalyst system combining Pd/TiO_2/HY with a conventional NH_3-SCR catalyst, Fe-BEA, achieved high NO conversion and with more than 90% N_2 selectivity between 180–300 °C also superior product selectivity. Spatially resolved concentration profiles in monolithic samples revealed that Fe-BEA mediates N_2O suppression and facilitates the rapid consumption of NH_3 species formed *in situ* over Pd/TiO_2/HY. These findings underscore the potential of advanced catalyst combinations to overcome current limitations of H_2-SCR and pave the way for cleaner hydrogen-based combustion technologies.

Received 19th November 2025,
Accepted 27th February 2026

DOI: 10.1039/d5cy01387a

rsc.li/catalysis

Introduction

On the way towards a decarbonization of the transport sector, lean-burn hydrogen internal combustion engines (H_2-ICE) represent a promising technology, as hydrogen combustion yields only water as a reaction product.[1,2] However, the elevated in-cylinder temperatures associated with hydrogen combustion promote the formation of thermal nitrogen oxides (NO_x), necessitating downstream catalytic abatement. In addition to established technologies like NO_x storage and reduction (NSR) catalysts (commonly Pt/BaO/Al_2O_3 or similar formulations) and selective catalytic reduction (SCR) of NO_x using ammonia (NH_3) provided through thermolysis and hydrolysis of urea–water solution (typically employing V_2O_5–WO_3–TiO_2 or Cu and Fe incorporated into zeolites as catalysts), the selective catalytic reduction of NO_x using hydrogen (H_2-SCR) gains increasing attention.[3–5] The inherent advantage of H_2-SCR lies in the direct utilization of hydrogen fuel as the reductant. Nevertheless, two major challenges impede its widespread adoption: the relatively low selectivity of the H_2-SCR reaction, which can lead to the formation of nitrous oxide (N_2O), a potent greenhouse gas, as well as toxic ammonia, and diminished catalytic activity at elevated temperatures due to the preferential oxidation of hydrogen by oxygen (O_2).

Catalyst formulation plays a critical role in modulating both the activity and selectivity of the H_2-SCR process. Among the elements that gained particular attention in recent years for their outstanding activity are platinum (Pt),[6] palladium (Pd),[7] and iridium (Ir).[8,9] A comparative study by Shao *et al.*[9] demonstrated that these metals exhibit optimal performance across distinct temperature regimes: Pt at low temperatures, Pd at intermediate temperatures, and Ir at high temperatures. Also, rhodium (Rh) has been tested in the past.[10] Among all these elements, Pd is particularly attractive due to its high activity in the medium-temperature range and its comparatively superior selectivity, especially when contrasted with the highly active but less selective Pt.[11] These attributes position Pd as a particularly

Institute for Chemical Technology and Polymer Chemistry, Karlsruhe Institute of Technology (KIT), 76131 Karlsruhe, Germany. E-mail: patrick.lott@kit.edu
† These authors contributed equally.

promising candidate for the development of H_2-SCR catalysts with broad operational temperature windows. It is noteworthy that optimal noble metal loadings vary significantly and are often closely linked to the specific catalyst formulation. This dependency arises from factors such as noble metal particle size, which commonly correlates with loading and specific surface area, and metal–support interactions, both of which critically influence catalytic performance.[12–15]

With regard to the support material, numerous studies have demonstrated that metal oxide supports significantly enhance catalytic performance, primarily by benefiting a reduced metallic noble metal state.[16–18] However, many studies also rely on zeolite materials, frequently combined with metal oxides in order to enhance the performance.[19–24] The addition of promoters has been demonstrated to be an effective strategy for enhancing both the activity and selectivity of H_2-SCR catalysts, with a wide range of promoter materials proposed in the literature. These include electron-donating alkali and transition metals, which are hypothesized to benefit reaction pathways relevant to H_2-SCR on the one hand and to stabilize the catalytically active metallic state of the noble metal component on the other hand.[25–28] Furthermore, tungsten oxide (WO_x) has been suggested not only to serve as a structural promoter but also to facilitate favorable SCR-related reaction pathways at the noble metal–support interface.[29–31] Vanadium oxide (V_2O_5, VO_x) has also been investigated for its potential to promote selective NO_x reduction, presumably by enabling the formation of beneficial NH_4^+ intermediates.[32–34]

The *in situ* formation and storage of such NH_4^+ intermediates is facilitated on catalyst formulations with a high number of acidic surface sites, which results not only in higher activity but also in higher selectivity toward nitrogen.[35] In a previous study by our group, the TiO_2/HY composite support was proposed as a particularly promising formulation for Pd-based catalysts, offering both reducible metal oxide and acidic sites.[36] This dual functionality facilitates high activity in the H_2-SCR reaction while maintaining favorable selectivity toward nitrogen.

As an initial step, the Pd loading was systematically varied to establish correlations between NO_x conversion, product selectivity, and metal loading. Subsequently, the influence of WO_3 and V_2O_5 additions on the catalytic performance was investigated. Given that NH_4^+ has been identified as a key intermediate not only in H_2-SCR but also in NH_3-SCR processes,[37] the H_2-SCR catalyst was ultimately combined with a conventional NH_3-SCR formulation, namely Fe-BEA, in a final step. While kinetic testing served as the primary method for evaluating the suitability of the catalyst formulations for H_2-SCR applications, complementary materials characterization enabled the establishment of structure–activity relationships. Additionally, the capillary-based spatial profiling (SpaciPro) technique was employed to obtain axially resolved concentration profiles of reactive species within monolithic catalyst channels, thereby providing mechanistic insights into the reaction pathways relevant to H_2-SCR.

Experimental

Catalyst materials

The first step in preparing the noble metal catalysts was a calcination of commercial Zeolite-Y (CBV300, Zeolyst) at 500 °C for 6 h in static air. Afterwards, TiO_2 was precipitated from a $Ti(OBu)_4$ solution in ethanol by dropwise addition of a H_2O/ethanol (1 : 1, v : v) solution. After drying at 70 °C for at least one hour, a second calcination step was conducted at 500 °C for 6 h in static air. For tungsten- or vanadium-containing catalysts, an incipient wetness impregnation was done to add WO_3 (from $(NH_4)_6H_2W_{12}O_{40}$, Fluka Analytics) or V_2O_5 (from NH_4VO_3 in an oxalic acid/water solution, Alfa Aesar), followed by another calcination step (6 h at 500 °C in static air). Finally, Pd was added from $Pd(NH_3)_4(NO_3)_2$ (abcr, 5.0%Pd solution) *via* incipient wetness impregnation and a final calcination at 500 °C for 6 h in static air. The iron zeolite was prepared from Zeolite Beta (Thermo Scientific) *via* ion exchange in an aqueous $FeSO_4$ solution with a pH of 2–3 at 80 °C and with stirring for 2 h.

While the majority of measurements presented herein were conducted with powder catalyst samples, some measurements were conducted with catalytically coated monolith samples (3.0 cm length, 97 cells, 400 cpsi; Corning) to mimic more realistic conditions and to enable spatial profiling (SpaciPro) experiments. First, a slurry was prepared by mixing the respective catalyst powder or a physical mixture of the catalyst powders with 10% of AlO(OH) (Disperal P2, Sasol) as binder in deionized water and acidification to pH 4 with HNO_3. The slurry was then added to the monolithic channels *via* dip-coating and excess liquid was blown out before drying with hot air. These steps were repeated until the target noble metal loading of 20 g ft^{-3} was achieved. The resulting sample was calcined in static air at 500 °C for 6 h. The monolith that contained two formulations was coated with a weight ratio of 2 : 1 of noble metal catalyst to iron zeolite.

Catalyst characterization

The exact elemental compositions of the catalyst powders were determined by inductively coupled plasma optical emission spectroscopy (ICP-OES). Surface area and pore volume of the different materials were determined *via* N_2 physisorption with a BELSORP-mini II instrument (BEL Japan). After 2 h of degassing at 300 °C, the N_2 adsorption–desorption isotherms were measured and subsequently evaluated with the method of Brunauer, Emmett, and Teller (BET).[38] Furthermore, X-ray diffraction (XRD) patterns were measured with a Bruker Advance D8 diffractometer using Cu-K_α radiation with a wavelength of 1.54 Å. The diffraction angle 2θ was scanned from 20° to 80° in steps of 0.016° with an acquisition time of 0.51 s per step. Temperature-programmed desorption of ammonia (NH_3-TPD) was performed using 100 mg of catalyst powder diluted with 900 mg of inert SiO_2 (both sieved to a particle size of 125–250 μm). Prior to adsorption, the samples were pretreated at 500 °C for 60 min under a flow of N_2 with a heating rate of 2 K min^{-1} to remove adsorbed species. After

cooling to 100 °C, ammonia adsorption was carried out at 100 °C using a gas mixture of 1000 ppm NH_3 in N_2 at a total flow rate of 1 L min^{-1}. Subsequently, the samples were purged with N_2 at 100 °C for 60 min to remove physisorbed NH_3. The NH_3-TPD experiment was then conducted by heating the samples from 100 °C to 650 °C at a rate of 2 K min^{-1} under a N_2 flow of 1 L min^{-1}. The amount of NH_3 desorbed during the TPD step was quantified based on Fourier-transform infrared spectrometer data (MultiGas 2030, MKS Instruments), and the total acidity was reported as μmol NH_3 per g catalyst. The Pd dispersion was obtained from CO chemisorption measurements following a procedure described previously.[39] In brief, the powder catalyst sample was fixed in a quartz glass tubular reactor, subjected to pretreatment (30 min in flowing air at 550 °C), and then completely reduced at 400 °C by 60 min exposure to a reductive gas flow (5 vol% H_2 in N_2). After cooling the reactor to ambient temperature under a continuous N_2 flow, the catalyst was exposed to a 1 vol% CO/N_2 mixture for 60 min to achieve surface saturation. Subsequently, the system was purged with N_2 to remove residual gaseous and physisorbed CO species. A temperature-programmed desorption (CO-TPD) experiment was then conducted under an inert N_2 atmosphere up to a final temperature of 550 °C (heating rate 20 K min^{-1}). Both the concentrations of CO and CO_2 were measured with an infrared spectrometer (X-Stream, Emerson); CO_2 may form through the reaction of CO with lattice oxygen or traces of O_2 due to impurities in the feed gas stream. The acquired data allow to determine the Pd dispersion under the assumption of an adsorption stoichiometry of 1 : 1.[40] Moreover, if a hemispherical nanoparticle size is assumed, the mean Pd particle size (d_{Pd}) can be calculated from the dispersion (D_{Pd}) according to eqn (1).[40]

$$d_{\text{Particle}} = \frac{1.11}{D_{\text{Pd}}} \quad (1)$$

Catalyst test bench and kinetic testing procedure

To compare the catalytic activity of the different catalyst formulations, dynamic light-off measurements were performed in a synthetic gas test bench. For the catalyst powders, a synthetic gas test bench described in detail already in earlier publications from our team[36,41] was used with 300 mg of catalyst powder diluted with 700 mg SiO_2, both in a size distribution of 125 μm to 250 μm (if not specified otherwise). The catalyst bed was packed into a quartz glass tubular reactor (inner diameter: 8 mm) and clamped with quartz glass wool. The feed gas was mixed from pure gases (provided by gas bottles, Air Liquide) using mass flow controllers (MFC, Bronkhorst) and a combination of a liquid flow controller (LFC, Bronkhorst) and a controlled evaporator mixer (CEM, Bronkhorst) that allowed to dose water vapor and thus enabled to simulate humid exhaust gas. Before the start of the activity tests, a degreening step was performed for 1 h at 500 °C in reaction gas mixture (1000 ppm NO, 5000 ppm H_2, 10 vol% O_2, and 10 vol% H_2O in N_2), followed by a preoxidation at 500 °C for 20 min with 10 vol% O_2 in N_2 that ensures a well-defined catalyst state prior to each catalyst test. Then, two consecutive light-off measurements between 100 °C and 300 °C were performed with a temperature ramp rate of 2 K min^{-1} in a water-free reaction gas mix (1000 ppm NO, 5000 ppm H_2, and 10 vol% O_2 in N_2) and after another oxidation step, the light-off procedure was repeated with a humid mix (1000 ppm NO, 5000 ppm H_2, 10 vol% O_2, and 10 vol% H_2O in N_2). Before and after each light-off-light-out-cycle, the gas mix was led through the bypass for 20 min in order to verify correct dosage and to determine the exact gas species concentrations. A Fourier-transform infrared (FTIR) spectrometer (MultiGas 2030, MKS Instruments) was used for gas analysis. Notably, the GHSV was kept constant at 60 000 h^{-1} by balancing with nitrogen at all times. Note that all temperatures reported for light-off experiments presented hereafter are the temperatures measured at the catalyst inlet. Under non-reactive conditions, temperature gradients between inlet and outlet are negligible across the entire temperature range relevant to this study (<0.5 °C). Despite the isothermal reactor characteristic under non-reactive gas flow, a temperature gradient of up to 10 °C is observed during the hydrogen light-off, which occurs due to the exothermic nature of the reactions involving H_2, in particular H_2 oxidation.

In addition to powder catalyst testing, spatially resolved analysis of the reaction system at 150 °C, 200 °C, and 250 °C as well as 12 h long-term measurements at 200 °C were performed on the monolithic samples at 75 000 h^{-1} using a custom-built synthetic gas setup,[42] which allows measurement of the end-of-pipe concentration as well as the concentration profile along the axial position of the monolith. While in previous studies from our team a mass spectrometer was used, the complex chemistry during H_2-SCR involves a variety of N-containing species whose simultaneous quantification by mass spectrometry is difficult. Thus, for the present experiments we used an FTIR spectrometer (MultiGas 2030, MKS Instruments) for spatial profiling (SpaciPro). During the spatially resolved measurements a sample volume flow rate of 29.6 ml min^{-1}, representing 45% of the nominal flow rate in a channel, is extracted from the monolith by means of a fused silica capillary (430 μm OD, 320 μm ID, 390 mm length, Polymicro), which occupies 12% of the cross-section of the channel. These values for nominal flow rate and channel cross-section are very similar to values reported previously by Hlavatý *et al.*,[43] who proposed the so-called balanced fast-SpaciMS method for a nominal flow rate of 43% and a channel cross-section of 11%. As the authors demonstrated reliability of spatially resolved data for their setup geometry, the similarity of our configuration enables us to determine accurate channel-averaged concentration profiles as well. To avoid long residence times in the 200 ml measuring cell of the FTIR analyzer, the gas sample obtained from within the monolith channel is diluted with nitrogen in a ratio of 1 : 9 before entering the spectrometer. Prior to the measurement of the spatially resolved profiles under dry or humid conditions, the sample underwent oxidation in 10 vol% O_2 in N_2 for 20 min at 500 °C, followed by three consecutive light offs from 100 °C to 300

°C with 2 K min^{-1}. Furthermore, prior to the measurement of each profile, the catalyst was subjected to the oxidation treatment described above. In contrast to the powder measurement and in order to prevent the condensation of water inside the capillary, SpaciPro measurements in the presence of steam were carried out using only 5 vol% H_2O instead of 10 vol% H_2O.

Results and discussion

Catalyst characterization

Compared to a TiO_2-free 1%Pd/HY catalyst from an earlier study that exhibited a BET surface area of 510 m^2 g^{-1},[36] the surface areas of the catalysts studied herein (Table 1) range from 171 m^2 g^{-1} (1%Pd/V_2O_5/TiO_2/HY) to 445 m^2 g^{-1} (1%Pt/WO_3/TiO_2/HY) and are thus generally reduced. While this can mainly be attributed to blockage of zeolitic pores by the precipitated TiO_2 layer, the surface area variations throughout the series of TiO_2-containing catalyst samples are likely linked to subtle differences in each individual synthesis. This is evident from the correlation between the measured acidity and the specific surface area (*cf.* Table 1). The observed linear relationship between acidity and BET surface area (Fig. S7) indicates progressive blockage of the zeolite pores during incipient wetness impregnation of the promoters and the noble metal. The Fe-BEA catalyst, on the other hand, exhibits a very high surface area of 666 m^2 g^{-1} after the ion exchange.

For the sake of clarity, the nominal compositions are used throughout this study to refer to the investigated catalyst samples. However, the precise contents of noble metals and promoters are detailed in Table 1. Although elemental analysis indicates slightly elevated noble metal concentrations compared to those expected based on the synthesis protocol, the relative trends across different loading levels remain consistent. This discrepancy may be attributed to the hygroscopic nature of the zeolite support, which could have influenced the accuracy of mass measurements during sample preparation.

XRD analysis (*cf.* Fig. S1–S3) reveals diffraction peaks exclusively associated with TiO_2 and Zeolite Y, suggesting a high degree of dispersion of the active metals, Pd and Fe, within their respective zeolitic frameworks. Notably, no diffraction signals corresponding to the promoter oxides WO_3 and V_2O_5 were observed. While this absence may also reflect a fine dispersion of these oxides, the relatively high loading levels (>5 wt%) suggest that these species may be present in an amorphous phase rather than in a crystalline form detectable by XRD.

Influence of noble metal loading

TiO_2/HY-supported catalysts with different palladium loading (0.1 wt%, 0.5 wt%, 0.75 wt%, and 1 wt%) were evaluated for their performance in a water-free (1000 ppm NO, 5000 ppm H_2, 10 vol% O_2 in N_2) and humid (1000 ppm NO, 5000 ppm H_2, 10 vol% O_2, 10 vol% H_2O in N_2) gas mixture. As underscored by the kinetic data depicted in Fig. 1, increasing the Pd-loading from 0.1 wt% to 0.5 wt% and 0.75 wt% shifts the NO light-off toward lower temperature, both in dry and humid conditions. While the 0.75 wt% Pd sample exhibits the highest NO_x conversion, the sample with a Pd loading of 1 wt% shows lower activity, at least for temperatures above 160 °C, despite the higher noble metal content. Taking the characterization data from Table 1 into account, our findings suggest an optimum palladium loading that is influenced by two key properties: the dispersion of the active species and the surface area of the catalyst. In general, an increasing noble metal loading typically results in larger particles, but only if the surface area is constant. Both 0.75%Pd/TiO_2/HY and 1%Pd/TiO_2/HY were found to have a dispersion ≤5%, corresponding to a mean Pd particle size of >22 nm. However, among the samples tested herein, 1%Pd/TiO_2/HY exhibits the lowest specific surface area (264 m^2 g^{-1}), whereas the most active 0.75 wt% Pd sample has a specific surface area of 339 m^2 g^{-1}. Since the NO reduction efficiency of Pd strongly correlates with the Pd particle size and since the noble metal–support interactions, which are commonly characterized by the interface of Pd and the support, strongly govern catalytic behavior,[44,45] we can assume a complex interplay of microscopic properties accounting for the performance maximum of the 0.75 wt% Pd catalyst. Moreover, the size of carbon-supported Pd particles was reported to determine the efficiency of nitrite reduction in aqueous environment both in terms of activity and product selectivity.[46] This is of particular importance in the context of

Table 1 BET surface area and pore volume obtained from N_2 physisorption measurements, Pd dispersion and Pd particle size obtained from CO-chemisorption measurements, and elemental compositions of the catalyst formulations determined by ICP-OES. Information on standard deviations can be found in the SI

Catalyst formulation	A_{BET} [m^2 g^{-1}]	V_{pore} [cm^3 g^{-1}]	Acidity [μmol g^{-1}]	Dispersion [%]	$d_{particle}$ [nm]	Active metal [wt%]	Promoter [wt%]	TiO_2 [wt%]	SiO_2 [wt%]	Al_2O_3 [wt%]
1%Pd/TiO_2/HY	264	0.16	320	5.0	22.4	1.25	—	23.6	55.2	19.9
0.75%Pd/TiO_2/HY	339	0.19	560	3.3	33.7	0.94	—	27.2	52.8	19.0
0.5%Pd/TiO_2/HY	417	0.19	560	12.6	8.8	0.62	—	27.1	53.0	19.3
0.1%Pd/TiO_2/HY	310	0.19	480	10.9	10.2	0.134	—	28.0	51.6	20.3
1%Pd/WO_3/TiO_2/HY	427	0.24	580	9.6	11.5	1.30	5.61	27.1	47.6	18.4
1%Pd/V_2O_5/TiO_2/HY	171	0.13	290	3.4	32.7	1.16	5.65	26.6	48.2	18.4
Fe-BEA	666	0.33	470	—	—	3.73	—	—	92.1	4.2

Active metal is either Pd or Fe; promoter is either WO_3 or V_2O_5.

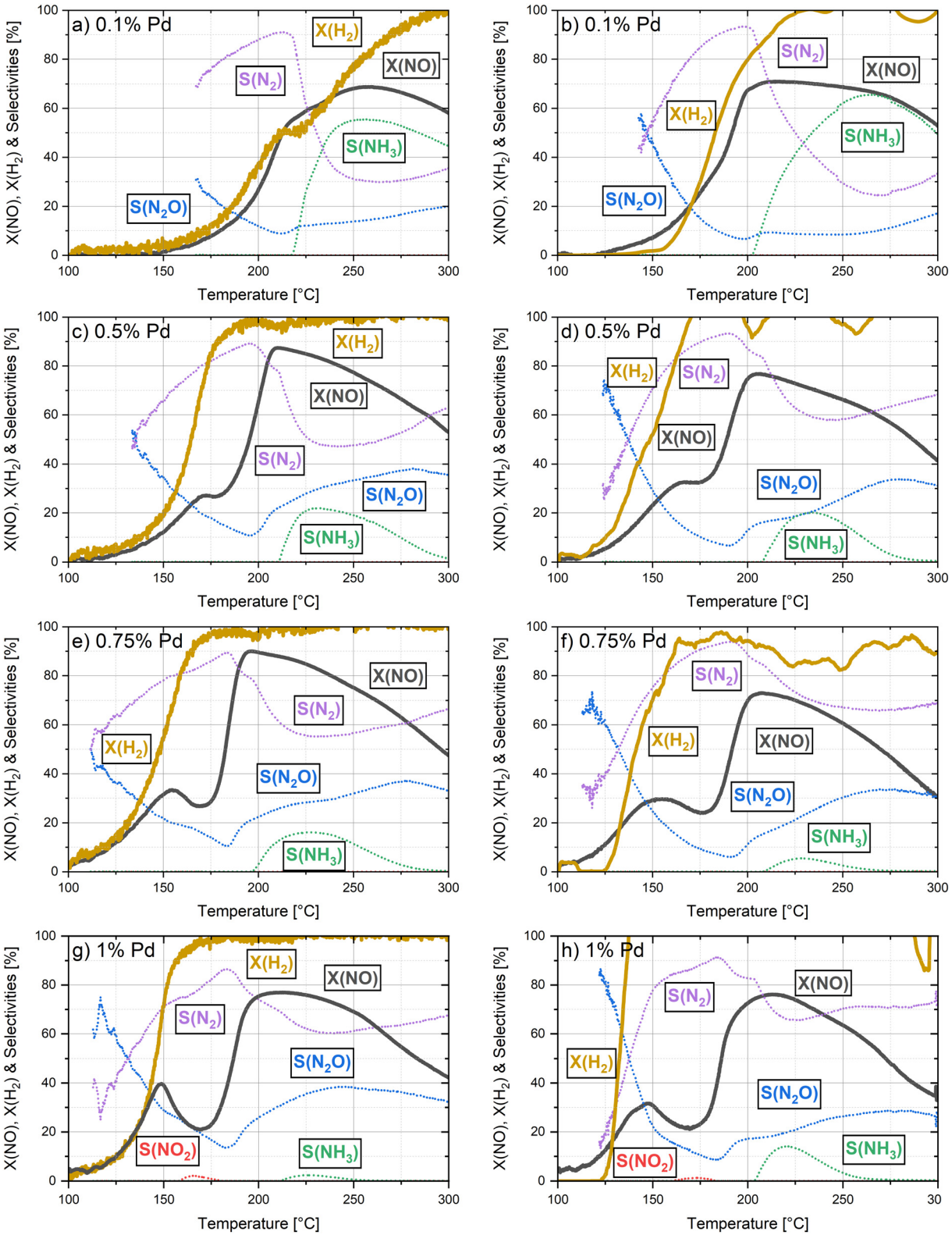

Fig. 1 NO and H_2 conversion (solid lines) and product selectivities (dotted lines) during the light-off measurements of the *x*%Pd/TiO_2/HY catalysts with *x* = 0.1 (a and b), 0.5 (c and d), 0.75 (e and f), and 1 (g and h) in the dry gas mixture (a, c, e and g; 1000 ppm NO, 5000 ppm H_2, 10 vol% O_2 in N_2) and humid gas mixture (b, d, f and h; +10 vol% H_2O); GHSV = 60 000 h^{-1}.

H_2-SCR, because species such as nitrates, nitrites, and nitro-compounds were reported to be formed and stored especially at the interface of PdO and TiO_2 under H_2-SCR conditions.[47] Not only the NO conversion, but also the dry (Fig. 1a, c, e and g)

and humid (Fig. 1b, d, f and h) hydrogen light-off is strongly affected by the noble metal loading: temperatures of 50% conversion (T_{50}) of 146 °C, 148 °C, 165 °C, and 210 °C under dry and 132 °C, 141 °C, 148 °C, and 182 °C under humid conditions were found for the samples with 1 wt%, 0.75 wt%, 0.5 wt%, and 0.1 wt% of palladium, respectively. Note that the H_2 conversion was determined from the H_2O signal recorded by the FTIR analyzer. Under humid feed conditions, fluctuations in the H_2O dosing resulted in increased experimental uncertainty and pronounced noise in the calculated H_2 conversion. Therefore, the data obtained in the presence of 10 vol% H_2O were post-processed using a 100-point moving-average filter. The validity of this data-processing approach was assessed using one representative experiment, in which the H_2 conversion derived from the FTIR data was independently verified by direct H_2 concentration measurements using a sector-field mass spectrometer (HSense, MS4 Analysentechnik). The calculated and directly measured H_2 light-off curves show good agreement, in particular in the vicinity of T_{50} (*cf.* Fig. S5).

Notably, the H_2 conversion also impacts the shape of the NO light-off curves. For Pd loadings of 0.75 wt% and 1 wt%, two NO conversion maxima are observed both in dry and humid conditions (Fig. 1e–h). The first one occurs at lower temperatures and strongly correlates with the onset of full H_2 conversion, whereas the second maximum typically occurs when according to the end-of-pipe data H_2 is already completely converted. This characteristic trend is in line with previously reported performance data, and based on their investigation on Pd/TiO_2-based H_2-SCR catalysts, Ueda *et al.*[48] suggested the two maxima to originate from different reaction paths: direct reduction of NO by H_2 at lower temperatures and reduction of *in situ* generated NO_2 by H_2 at higher temperatures. While we found that the second NO conversion maximum occurring at temperatures above 180 °C becomes flatter and broader upon loading reduction, we cannot draw profound conclusions on the high-temperature mechanism. However, we can confirm the low-temperature mechanism suggested by Ueda *et al.*[48] If the Pd loading is decreased to only 0.1 wt%, the local low-temperature maximum in the conversion curve vanishes entirely, which directly correlates with insufficient H_2 activation in the low-temperature regime. Furthermore, the shape of the NO_x conversion curves in dry and humid conditions is similar, which points to a NO_x conversion mechanism that is not majorly biased by the presence of steam. However, irrespective of the Pd loading, the overall NO_x conversion is generally suppressed in the presence of 10 vol% H_2O, which we attribute to competitive adsorption of NO_x, H_2, and H_2O. Zhao *et al.*[22] investigated Pt/HZSM-5 catalysts for H_2-SCR and suggested a temperature-dependent H_2O effect. They suggested a promotion of NO_x conversion below 120 °C and a suppression of NO_x conversion above 120 °C and explained it through a suppression of NO surface adsorption in both regimes: while lower NO surface coverage allows for more efficient H_2 activation in the low-temperature regime, it facilitates the combustion of the reducing agent H_2 at higher temperatures. Although the different catalyst formulation chosen in this study impedes a direct transfer of this interpretation, we can expect the same effects coming into play over the Pd-based catalysts subject to this study, yet with different temperature regimes.

In addition to the H_2 and NO conversion, also the product selectivity changes with the loading. In water-free reaction environment, a progressively higher ammonia formation is observed if the Pd loading decreases (Fig. 1a, c, e and g). In contrast, the N_2O selectivity is lowest for the 0.1 wt% palladium catalyst, but rises with increasing Pd loading. The highest selectivity to N_2, which is the desired product, can be achieved with the highest loading (Fig. 1g). When mimicking more realistic H_2-ICE exhausts by addition of 10 vol% H_2O, the trends become less straight-forward. Compared to the dry reaction gas mixture, even more ammonia is formed, with a maximum NH_3 selectivity of 66% at 265 °C for the 0.1%Pd/TiO_2/HY catalyst (Fig. 1b). Furthermore, N_2O formation is generally promoted by the presence of steam in the low-temperature regime, where NO conversion is low, but slightly suppressed for moderate and high temperatures ($T >$ 160–170 °C). The selectivity toward the target product N_2 is slightly higher in humid conditions and, equally important, the temperature window with reasonably high N_2 selectivity is broader in humid conditions. Note that NO_2 formation took place only over 1%Pd/TiO_2/HY, which suggests that a sufficiently high loading is required for oxidation of NO, whereas lower loadings favor the reduction of NO. Also, the higher noble metal loading seems to increase the robustness of the catalyst toward humidity, since the maximum NO conversion drop is less pronounced for 1%Pd/TiO_2/HY than, *e.g.*, for 0.75%Pd/TiO_2/HY.

To facilitate a direct comparison of the performance and to elucidate the interplay of H_2 activation and NO conversion in greater detail, turnover frequencies (TOFs) were calculated for all catalysts operated in dry reaction environment. For this, the data plotted in Fig. 1a, c, e and g were used in order to calculate the TOF for H_2 conversion as well as NO conversion according to eqn (2).

$$\mathrm{TOF} = \frac{\frac{p_0 \dot{V}_0}{RT_0} x_{\mathrm{i},0} X_\mathrm{i}}{\frac{m_\mathrm{Pd}}{M_\mathrm{Pd}} D_\mathrm{Pd}} \tag{2}$$

Herein, p_0, T_0 and $\dot{V}_0$ refer to the pressure, temperature, and total volumetric flow rate under standard conditions; $x_{\mathrm{i},0}$ and X_i denote the initial concentration and the conversion of H_2 and NO, respectively; m_Pd, M_Pd and D_Pd represent the total mass, molar mass, and dispersion of palladium, respectively.

In accordance with the absolute conversion data plotted in Fig. 1, the TOF data depicted in Fig. 2 underscore that the noble metal particle size alone is insufficient to determine catalytic activity. The highest turnover frequencies for both NO and H_2 conversion were found for the least active sample,

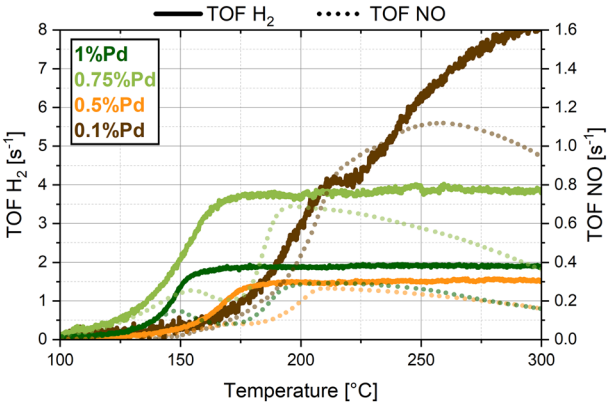

Fig. 2 Turnover frequency (TOF) for H_2 conversion (solid lines, left *y*-axis) and NO conversion (dotted lines, right *y*-axis) during the light-off measurements of the Pd/TiO_2/HY catalysts with different Pd loading in the dry gas mixture (1000 ppm NO, 5000 ppm H_2, 10 vol% O_2 in N_2); GHSV = 60 000 h^{-1}.

0.1%Pd/TiO_2/HY, notably, at temperatures exceeding 200 °C. Despite a slightly higher Pd dispersion of 12.6% and an even greater specific surface area, the 0.5%Pd/TiO_2/HY sample exhibits much lower TOF values and is outperformed by any other sample tested herein in terms of atom efficiency. Consistent with the activity data presented in Fig. 1, 0.75%Pd/TiO_2/HY exhibits the highest TOF values overall. The maximum TOF for NO conversion of 0.7 s^{-1} is found at approx. 195 °C, which coincides with the peak absolute NO conversion of about 90% (Fig. 1e). For H_2 activation, TOF values of approx. 4 s^{-1} are found once complete H_2 conversion is reached, with a plateau beyond 195 °C. Conversely, despite its higher noble metal loading, generally lower TOF values are observed for 1%Pd/TiO_2/HY, and the maximum TOF for NO (~0.3 s^{-1}) is found at around 213 °C, matching the maximum NO conversion of 77% (Fig. 1g). Given that CO chemisorption data indicate similar Pd dispersion for 1%Pd/TiO_2/HY (5%) and 0.75%Pd/TiO_2/HY (3.3%), other physicochemical parameters such as specific surface area (264 m^2 g^{-1} for 1%Pd/TiO_2/HY *versus* 339 m^2 g^{-1} for 0.75%Pd/TiO_2/HY) likely account for the observed differences in TOF data. As elaborated later, aspects like surface acidity play a critical role in H_2-SCR. Since the differences in surface area correlate with the number of acid surface sites available for adsorption of intermediate species, the surface area can impact the overall catalytic performance.

Addition of promoter materials

Since previous research pointed to a performance improvement if H_2-SCR catalyst formulations were modified with promoter materials such as WO_3 or V_2O_5, their addition to Pd/TiO_2/HY was evaluated in a next step. Compared to 1%Pd/TiO_2/HY (Fig. 1g), the addition of WO_3 results in a clear increase in activity in both the low- and high-temperature regime for the dry mixture (Fig. 3a). In particular, the T_{50} for hydrogen conversion is shifted toward lower temperatures, namely from 146 °C to 129 °C, and also the low-temperature NO conversion peak is shifted from 149 °C to 136 °C. Between 175 °C and 300 °C – the high-temperature regime – the activity for NO reduction is consistently higher as well. Only in the narrow temperature window between the two peaks (around 160 °C) the NO conversion falls below the levels of the unpromoted Pd catalyst by a small margin. The overall activity boost is assumed to originate from the electronic interaction between WO_3 and the noble metal; in analogy to what has been reported for WO_3-promoted Pt/TiO_2 H_2-SCR catalysts,[49] we can speculate about a higher share of metallic palladium sites (Pd^0) upon the introduction of WO_3. This is of high relevance because reduced palladium has been observed to be more active for the H_2-SCR reaction than palladium oxide for various Pd-based catalyst formulations.[27,41,50] With regard to product selectivity, the WO_3-promoted catalyst shows negligible ammonia formation and a slightly higher NO oxidation than the unpromoted one during the transition between the two NO conversion maxima around 160 °C. Nevertheless, N_2 and N_2O selectivities are overall comparable.

The addition of water to the reaction gas mixture does not alter these general trends significantly, although NO reduction efficiency below 150 °C is reduced to relevant extent in humid conditions (Fig. 3b). In contrast to the unpromoted 1%Pd/TiO_2/

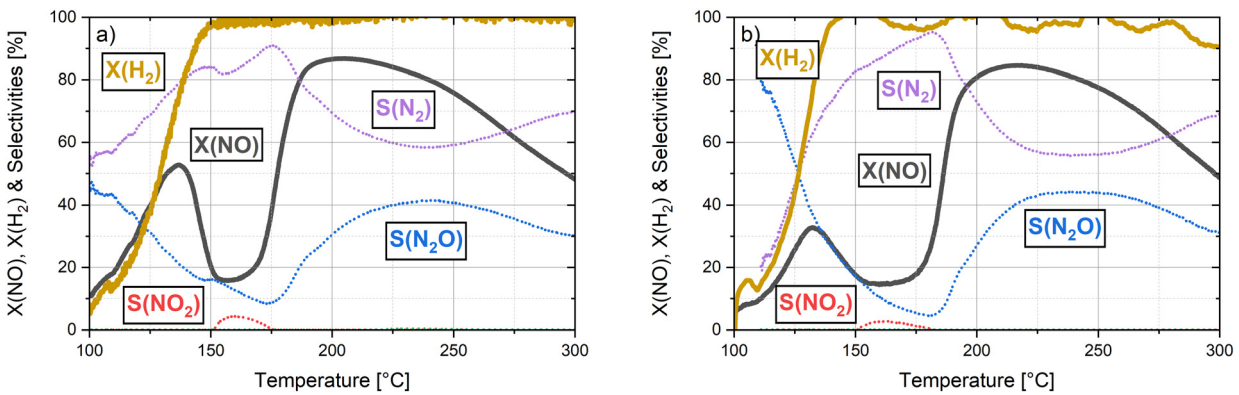

Fig. 3 NO and H_2 conversion (solid lines) and product selectivities (dotted lines) during the light-off measurements of the 1%Pd/WO_3/TiO_2/HY catalyst in the dry gas mixture (a, 1000 ppm NO, 5000 ppm H_2, 10 vol% O_2 in N_2) and humid gas mixture (b, +10 vol% H_2O); GHSV = 60 000 h^{-1}.

HY (Fig. 1h), NH_3 formation was found irrelevant over 1%Pd/WO_3/TiO_2/HY (Fig. 3b) and the presence of H_2O did not reduce the selectivity to the undesired product N_2O, but increased it even slightly for temperatures of 190 °C and above. Thus, despite promising performance of 1%Pd/WO_3/TiO_2/HY in dry environment and higher NO_x conversion than its unpromoted counterpart once temperatures exceed 180 °C, the fact that in real-world applications humidity will be omnipresent calls for further optimization of the catalyst formulation in order to suppress the generation of the strong greenhouse gas N_2O.

To address the need for enhanced selectivity in NO_x reduction, vanadium oxide (V_2O_5, VO_x) was tested as an alternative promoter, since it has been reported to facilitate the formation of NH_4^+ intermediates that presumably promote selective catalytic reduction pathways.[32–34] Although the performance data shown in Fig. 4 show that the selectivity of 1%Pd/V_2O_5/TiO_2/HY toward the target product N_2 can compete with that of the unpromoted 1%Pd/TiO_2/HY (Fig. 1g and h) sample both in dry and humid conditions, the addition of V_2O_5 results in a dramatic drop in catalytic activity especially in the presence of water (Fig. 4b). Considering the very low specific surface area (171 m^2 g^{-1}) of the vanadia-containing catalyst sample, we can speculate about a blockage of zeolitic pores and thus a reduction of acidic surface sites due to the addition of non-zeolitic material.[36] The NH_3-TPD-derived acidity data (*cf.* Table 1) support this hypothesis. Considering that NO reduction over noble metals such as Pt and Pd has been claimed to follow an NH_4^+-mediated reaction mechanism,[20,33,35] a lower number of Brønsted acid sites suppresses the formation of NH_4^+-species that could then react with NO_x to form N_2, hereby impeding efficient NO_x reduction. Taking the low dispersion of 3.4% (*cf.* Table 1) into account, we can also speculate about a partial blockage of highly active Pd^{2+} sites. Such Pd^{2+} ions can form as highly dispersed species in the sodalite cages of HY materials[51] and are believed to contribute to the overall NO_x conversion during H_2-SCR as well as to preserve high activity under humid conditions.[36] In conclusion, while we acknowledge the beneficial contribution of V_2O_5 to the N_2 selectivity, a simple deposition of vanadia onto high surface area supports as conducted herein has proven insufficient for H_2-SCR catalysts. However, advanced preparation techniques that allow for a more precise control of vanadia distribution on structured support materials may result in better performance.[34]

Combining H_2-SCR and NH_3-SCR catalyst formulations

Based on the data discussed thus far, the formation of the strong greenhouse gas N_2O constitutes a significant limitation in the implementation of H_2-SCR for NO_x abatement. To mitigate N_2O emissions during NO_x reduction *via* hydrogen, the integration of a secondary catalytic system capable of N_2O decomposition presents a viable strategy. Among the catalyst formulations reported in the literature, ion-exchanged iron zeolites – in particular Fe/ZSM-5 and Fe-BEA – have demonstrated relatively low activation temperatures for the N_2O decomposition reaction.[52,53] In addition, Fe-BEA was reported to catalyze NO reduction and N_2O decomposition simultaneously,[54,55] making it particularly promising for combination with H_2-SCR catalyst formulations prone to N_2O formation. To reconcile these findings with the need for hydrothermal stability under SCR conditions typical for H_2-ICE exhausts with high levels of humidity, Fe-BEA was selected as the more robust catalyst formulation.[56] This choice aims to minimize the N_2O levels while maintaining reasonable structural integrity under highly humid operational conditions. However, given that effective N_2O conversion requires temperatures exceeding 200 °C, the Pd-based H_2-SCR catalyst and the Fe-BEA catalyst were combined in a mechanical mixture rather than arranged sequentially. This configuration enables direct utilization of local temperature increases resulting from the exothermic total oxidation of hydrogen in the presence of oxygen. Throughout the tests discussed in the following, the catalyst bed was composed of 300 mg of Pd-based H_2-SCR catalyst, 300 mg of Fe-BEA catalyst, and 400 mg of SiO_2 as a diluent (reduced from the previously used 700 mg) to maintain a constant total mass of 1000 mg. Note that 1%Pd/TiO_2/HY was chosen over 0.75%Pd/TiO_2/HY for its superior water tolerance, which is particularly critical when evaluating the performance of the material combination under realistic humid conditions.

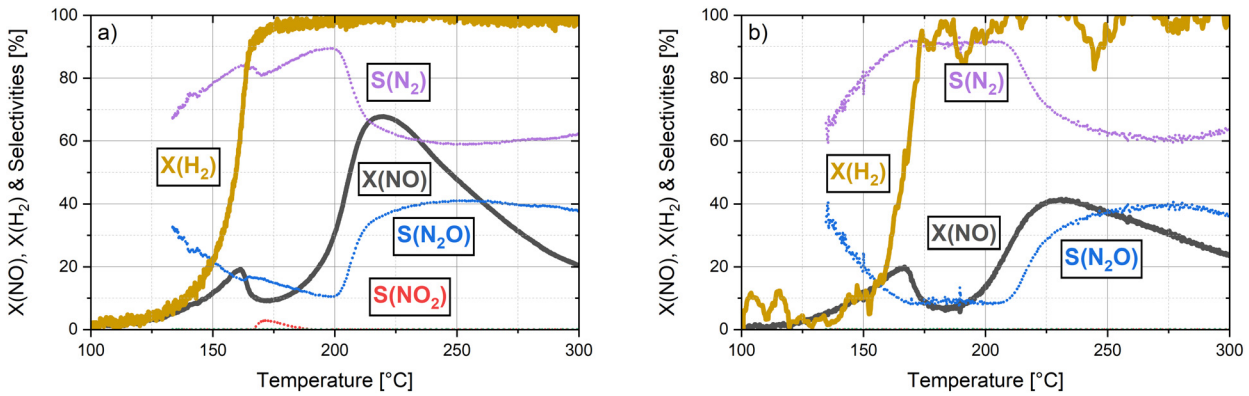

Fig. 4 NO and H_2 conversion (solid lines) and product selectivities (dotted lines) during the light-off measurements of the 1%Pd/V_2O_5/TiO_2/HY catalyst in the dry gas mixture (a, 1000 ppm NO, 5000 ppm H_2, 10 vol% O_2 in N_2) and humid gas mixture (b, +10 vol% H_2O); GHSV = 60 000 h^{-1}.

The data depicted in Fig. 5a indicate that the combination of 1%Pd/TiO_2/HY and Fe-BEA in a 1 : 1 mass ratio exhibits substantial NO conversion in the dry gas mixture at temperatures exceeding 180 °C, reaching a peak conversion of 92% at 213 °C. The hydrogen light-off for this catalyst combination is slightly shifted to higher temperatures, with a T_{50} of 153 °C, compared to 146 °C observed for the H_2-SCR catalyst alone. Overall, a markedly lower N_2O selectivity, and consequently enhanced N_2 selectivity, was observed for the combined catalyst system. However, at temperatures exceeding 250 °C, an increase in NO oxidation activity appears to occur, leading to a decline in N_2 selectivity due to the formation of NO_2. While this effect is particularly pronounced in dry reaction environment (Fig. 5a), humidity mitigates NO_2 evolution (Fig. 5b). In the presence of water vapor, N_2 selectivity remains above 90% across the high-activity temperature range of 180–300 °C. Despite a slight overall shift of NO conversion toward higher temperatures in the presence of water vapor, which we attribute to competitive adsorption of H_2O and surface hydroxyl groups on the active sites, the high selectivity toward N_2 remains particularly encouraging. This observation is of practical relevance, as real-world exhaust gas streams typically contain substantial levels of water vapor. Therefore, the robustness of N_2 selectivity under humid conditions underscores the potential applicability of the catalyst system in realistic operating environments.

It is also noteworthy that no ammonia was detected in the effluent gas stream when employing the combined Pd-based H_2-SCR and Fe-BEA catalyst system. This observation may be attributed to two factors. First, iron-exchanged zeolites are well-established NH_3-SCR catalysts and may facilitate *in situ* consumption of NH_3 generated within the catalyst bed for NO reduction.[57–59] Second, NH_3 can react with N_2O in the presence of iron zeolites,[60] hereby potentially representing another relevant reaction pathway, particularly at elevated temperatures.

Due to the significantly lower gravimetric density of Fe-BEA compared to the SiO_2 diluent, the catalyst bed length increased in the mixed catalyst configuration used in the aforementioned experiments. To eliminate potential effects arising from increased residence time, a second sample was prepared consisting of 300 mg of Pd-based catalyst and 215 mg of Fe-BEA, without any diluent. This configuration maintained the same bed length as that used in measurements with the H_2-SCR catalyst alone. The corresponding results, presented in the SI (Fig. S4), confirm the previously described trends. Notably, in contrast to the diluted mixture, hydrogen conversion in the undiluted system is shifted toward lower temperatures (Fig. S4), which may be attributed to elevated intra-catalyst temperatures resulting from reduced thermal dissipation in the absence of the diluent.

Mechanistic considerations derived from experiments with spatial resolution

Although the Pd-based catalyst likely continues to generate relevant quantities of ammonia or ammonium intermediates during the NO reduction process, no NH_3 was detected at the outlet of the catalytic bed comprising both Pd- and Fe-based components. This absence is presumably due to the rapid consumption of NH_3 *via* reactions with NO, NO_2, or N_2O over the Fe-BEA catalyst. To elucidate the complex interplay of reactions occurring within this bifunctional catalytic system and to identify the specific reactions involved, spatially resolved concentration measurements were performed. These measurements were conducted on monolithic samples coated either with 1%Pd/TiO_2/HY alone or with a combination of 1%Pd/TiO_2/HY and Fe-BEA in a 2 : 1 mass ratio. Note that this mass ratio differs from that of the powder catalyst tests; due to the above-mentioned low gravimetric density of Fe-BEA, a reduction of its content was necessary in order to achieve a reasonable washcoat thickness (approx. 35 μm) that keeps the relevance of internal diffusion low. To ensure catalyst stability during spatially resolved steady-state measurements, both the Pd-based and Fe-based catalysts were subjected to a 12-hour long-term test at 200 °C and a gas hourly space velocity (GHSV) of 75 000 h^{-1} under both dry and humid conditions.

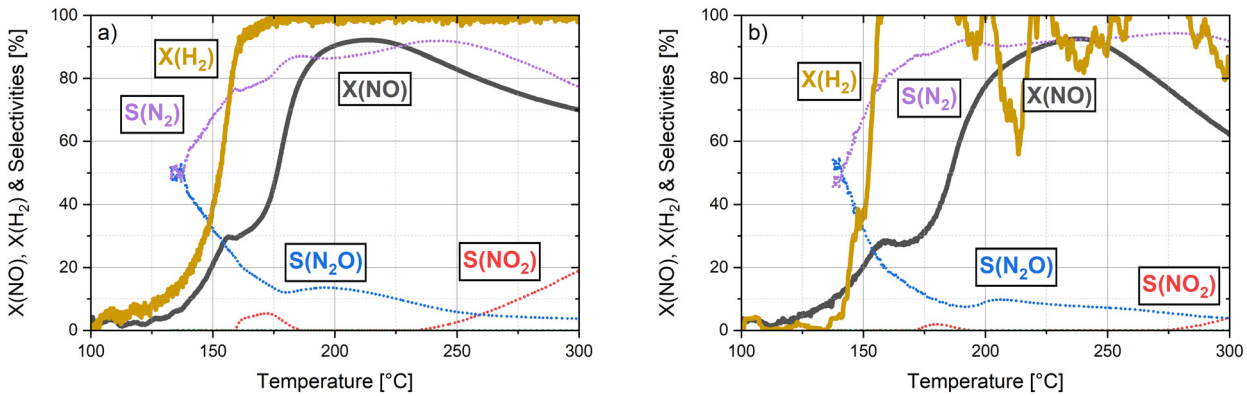

Fig. 5 NO and H_2 conversion (solid) and product selectivities (dotted lines) during the light-off measurements of the combination of 1%Pd/TiO_2/HY and Fe-BEA (1 : 1, m : m) catalysts in the dry gas mixture (a, 1000 ppm NO, 5000 ppm H_2, 10 vol% O_2 in N_2) and humid gas mixture (b, +10 vol% H_2O); GHSV = 60 000 h^{-1}.

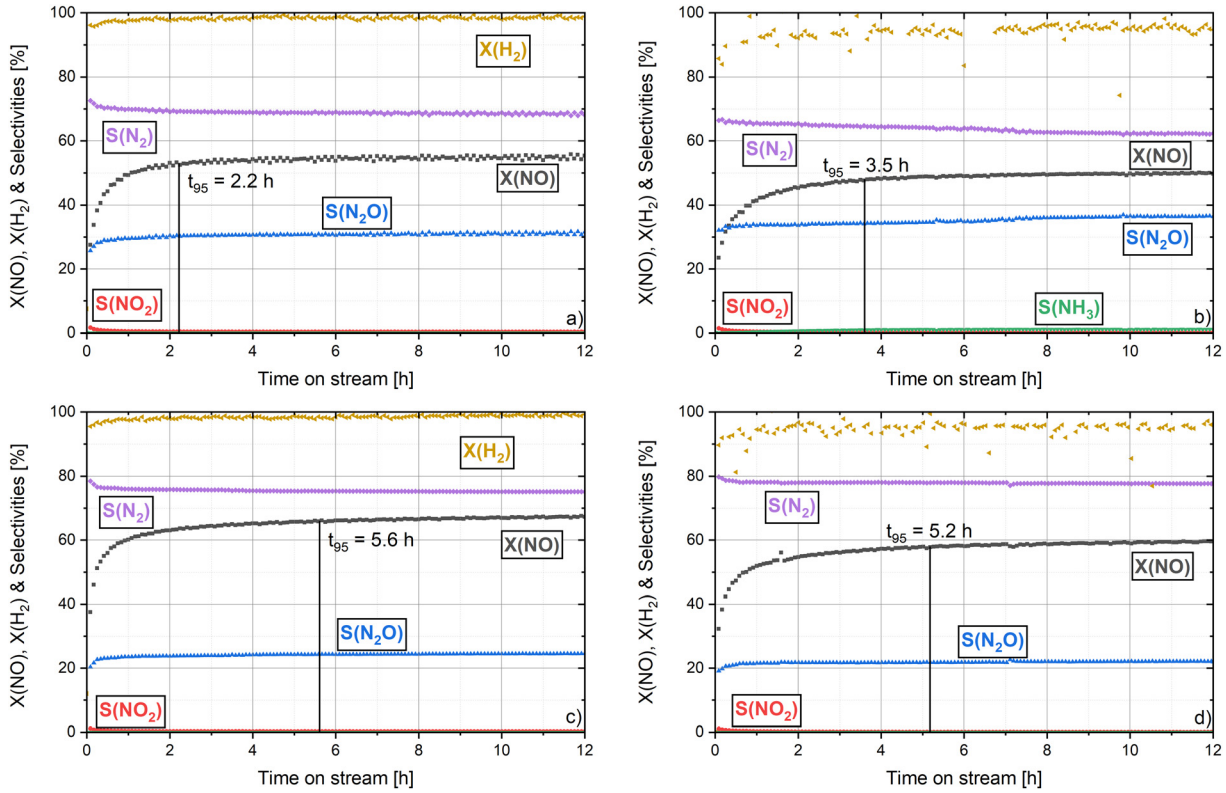

Fig. 6 Long-term trends of NO, H_2 conversion, and product selectivities of 1%Pd/TiO_2/HY (a and b) and 1%Pd/TiO_2/HY + Fe-BEA (2 : 1, m : m) (c and d) in the dry gas mixture (a and c: 1000 ppm NO, 5000 ppm H_2, 10 vol% O_2 in N_2) and humid gas mixture (b and d: +5 vol% H_2O) at a GHSV = 75 000 h^{-1} and T = 200 °C.

As shown in Fig. 6, all monolithic samples exhibited lower NO conversion under steady-state conditions compared to the light-off measurements conducted with powder samples. This observation is consistent with the higher GHSV employed in the long-term and spatially resolved experiments with monolithic samples, which results in reduced contact time between the gas and the catalyst surface. Also, the different mass ratio of 1%Pd/TiO_2/HY and Fe-BEA is expected to contribute to such variations. Furthermore, it is plausible that despite the low temperature ramp rate of 2 K min^{-1} as chosen herein, light-off measurements may not accurately reflect true steady-state performance at a given temperature. This discrepancy may arise from the catalytic system's relaxation time exceeding the characteristic time of the temperature ramp, thereby preventing full equilibration before data acquisition. More importantly, the catalysts demonstrated stable performance during the 12-hour exposure to the reaction gas mixture, with no observable loss in activity. In fact, NO conversion increased over time. For the Pd-based H_2-SCR catalyst alone, 95% of the steady-state NO conversion (t_{95}) – the steady-state NO conversion is defined as the absolute conversion achieved after 12 h – was reached after 2.2 h under dry conditions (Fig. 6a) and 3.5 h under humid conditions (Fig. 6b). In contrast, the physical mixture of the Pd catalyst and Fe-BEA required 5.6 h and 5.2 h to reach t_{95} under dry (Fig. 6c) and humid conditions (Fig. 6d), respectively.

Despite the differing space velocities employed in the powder and monolith experiments, which account for the lower NO conversion during spatial profiling, the observed trends remained consistent. Specifically, water vapor exposure led to a reduction in NO conversion and an increase in N_2O selectivity for the Pd-only catalyst (*cf.* Fig. 1g and h and 6a and b), whereas the Pd/Fe mixed catalyst exhibited a decrease in N_2O selectivity under the same conditions (*cf.* Fig. 5 and 6a and b). Additionally, NH_3 formation was detected in the effluent of the pure Pd catalyst under humid conditions (*cf.* Fig. 1h and 6b), while no ammonia was observed in the end-of-pipe measurements for both the powder and the monolithic 1%Pd/TiO_2/HY + Fe-BEA (2 : 1, m : m) catalyst under either dry or humid conditions (*cf.* Fig. 5 and 6c and d).

Fig. 7 presents the spatially resolved concentration profiles of NO, H_2, and reaction products along the monolith channel at temperatures of 150 °C, 200 °C, and 250 °C, at a GHSV of 75 000 h^{-1}. In analogy to the light-off tests discussed above, measurements were conducted under both dry (Fig. 7a–c) and humid (Fig. 7d–f) conditions using a monolithic 1%Pd/TiO_2/HY catalyst. At 150 °C, the NO reduction activity is minimal under both dry and humid conditions, with NO conversion not exceeding 10%. The predominant reaction products are N_2O and N_2, with some NO_2 detected as well, consistent with data at this temperature from light-off experiments. It is important to note that the quantification of H_2 was indirectly inferred by balancing with H_2O measurements obtained *via* FTIR

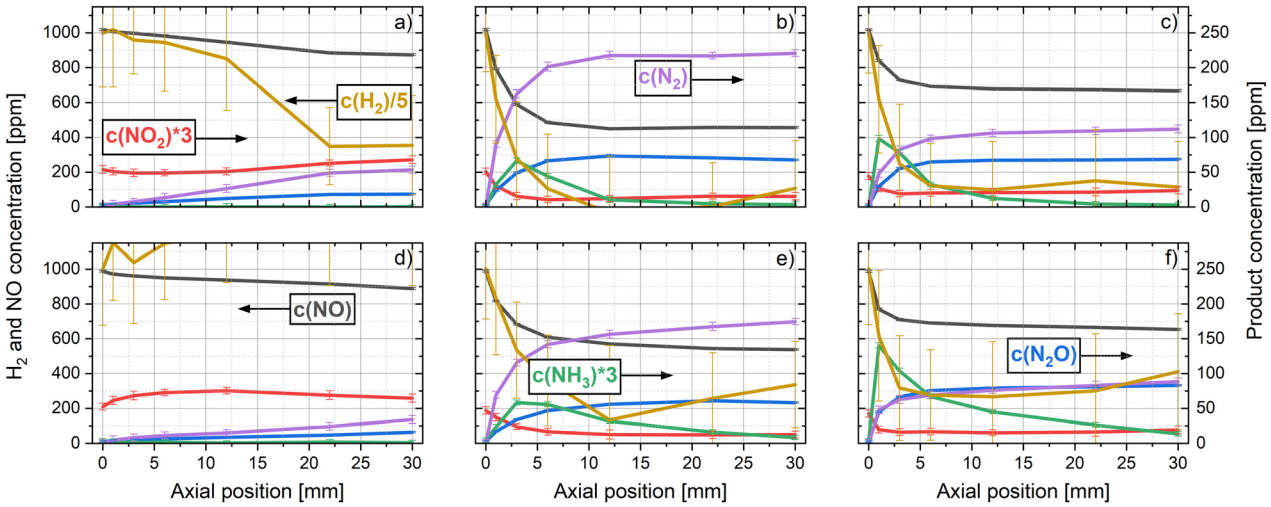

Fig. 7 NO, H_2, and product concentration profiles of the 1%Pd/TiO_2/HY monolithic catalyst in the dry gas mixture (a–c: 1000 ppm NO, 5000 ppm H_2, 10 vol% O_2 in N_2) and humid gas mixture (d–f: +5 vol% H_2O) at T = 150 °C (a and d), T = 200 °C (b and e), and T = 250 °C (c and f); GHSV = 75 000 h^{-1}.

spectroscopy. This approach introduced significant uncertainty due to the low signal-to-noise ratio of the H_2O signal. Furthermore, the additional dilution with N_2 during spatially resolved measurements exacerbated the signal degradation across all species. At 200 °C, the NO conversion reaches its maximum, in agreement with light-off data. The small amount of NO_2 observed at the catalyst inlet (~16 ppm) is fully consumed. In addition to the formation of N_2O and N_2, NH_3 is detected in the early segment of the catalytic channel. For example, under dry conditions, a peak NH_3 concentration of 22 ppm is observed approximately 3 mm downstream from the channel inlet (Fig. 7b), followed by its subsequent consumption along the channel length. At 250 °C, NO conversion declines due to competitive reduction reactions involving O_2 and NO with H_2. Nevertheless, NH_3 formation increases, with the peak concentration rising to 32 ppm and shifting closer to the channel inlet (Fig. 7c), indicating enhanced NH_3 formation at elevated temperatures. Due to limitations in spatial resolution, the true peak NH_3 concentration cannot be precisely determined. However, while the presence of water vapor does not appear to significantly alter the position or magnitude of the NH_3 peak, H_2O seems to inhibit NH_3 consumption, resulting in a minor NH_3 slip at both 200 °C and 250 °C under humid conditions.

Fig. 8 illustrates the spatially resolved concentration profiles for the bifunctional catalyst system 1%Pd/TiO_2/HY + Fe-BEA (2 : 1, m : m) under identical experimental conditions. At 150 °C, both dry and humid environments yield approximately 10% NO

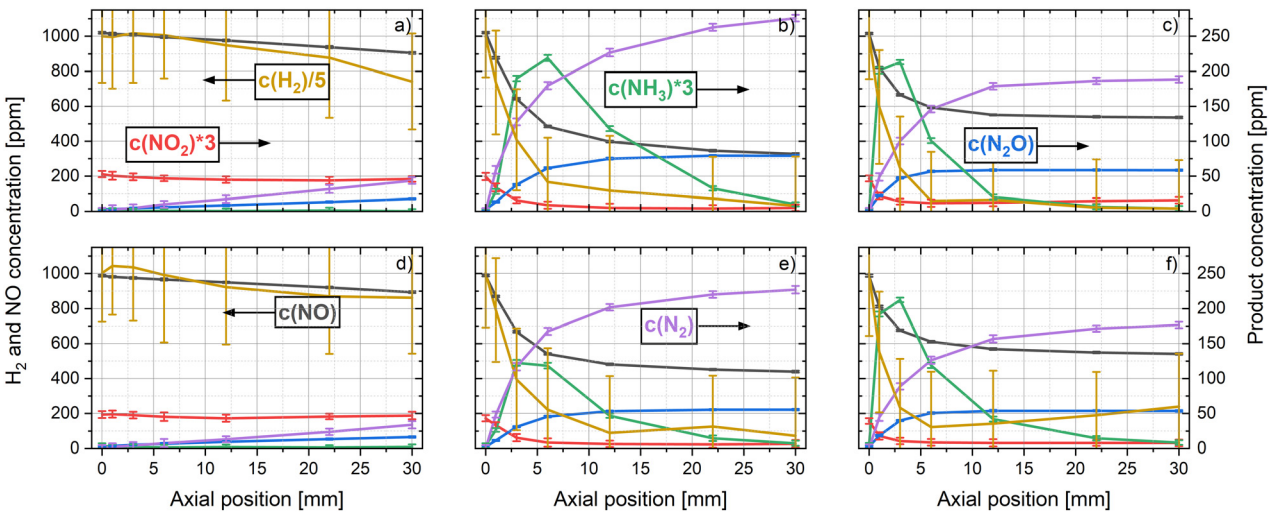

Fig. 8 NO, H_2, and product concentration profiles of the 1%Pd/TiO_2/HY + Fe-BEA (2 : 1, m : m) monolithic catalyst in the dry gas mixture (a–c: 1000 ppm NO, 5000 ppm H_2, 10 vol% O_2 in N_2) and humid gas mixture (d–f: +5 vol% H_2O) at T = 150 °C (a and d), T = 200 °C (b and e), and T = 250 °C (c and f); GHSV = 75 000 h^{-1}.

conversion, similar to the monofunctional 1%Pd/TiO_2/HY catalyst. The primary reaction products are N_2 and N_2O, while NO_2 concentrations exhibit a slight decline; however, this change remains within the margin of experimental error. At 200 °C, the NO conversion reaches its peak both in dry and humid conditions, with clearly enhanced N_2 formation compared to the monofunctional catalyst (*cf.* Fig. 7b and e and 8b and e). This improvement in both activity and selectivity is attributed to the incorporation of Fe-BEA. Zeolite-incorporated iron is known to be active for selective NO reduction in the context of conventional NH_3-SCR, where not H_2 but NH_3 serves as reducing agent,[61] and Fe-BEA in particular was found feasible for catalyzing simultaneous NO and N_2O reduction by NH_3.[54,55] Notably, compared to the monofunctional catalyst, a significantly higher NH_3 peak concentration of 73 ppm is observed over the bifunctional catalyst near the channel inlet (Fig. 8b). This increase is likely due to the presence of the zeolitic BEA support, which introduces a greater density of Brønsted acid sites and thereby facilitates the formation of NH_4^+ intermediates.[62] Their decomposition into NH_3 and subsequent desorption may account for the increased NH_3 levels. Moreover, the direct interaction of Fe and Pd-based catalysts within the washcoat may enhance desired reaction pathways. Dong *et al.*[63] investigated Pt/SSZ-13 formulations for their NO reduction efficiency when using H_2 as reductant and concluded that two reaction pathways occur in H_2-SCR conditions: (i) the formation of NH_x^+ species, in particular NH_4^+, and their subsequent oxidation with high selectivity towards the desired reaction product N_2; (ii) the catalytic reduction of NO by NH_3 and thus conventional NH_3-SCR-like reactions taking place on noble metal-based materials, yet with comparably poor selectivity and thus formation of high N_2O levels. In this regard, the promotion of NH_4^+ intermediate formation as well as the NH_3-SCR reaction taking place over Fe with higher selectivity than over noble metal particles could explain the overall better performance of the sample washcoated with the material mixture compared to the sample coated with Pd/TiO_2/HY only. This hypothesis is substantiated by the spatially resolved measurements, which uncover that the bifunctional catalyst formulation effectively converts the elevated NH_3 concentrations formed at the inlet, which we attribute to NH_3-SCR reaction pathways taking place over Fe sites and hereby promote the overall NO_x reduction efficiency. Similar to the trends observed for the monofunctional catalyst, the NH_3 concentration peak shifts upstream toward the channel entrance at 250 °C, indicating temperature-dependent NH_3 formation dynamics. In contrast to 1%Pd/TiO_2/HY, the addition of water does not appear to impair the NH_3 conversion efficiency of the bifunctional catalyst (Fig. 8e and f). This suggests that the addition of the Fe-BEA component improves robustness in the presence of water, likely due to enabling NH_3-SCR reaction pathways. Water vapor can promote these through a hydroxyl-induced transformation of Lewis acid sites into Brønsted acid sites that enable higher surface coverage of important intermediates, in particular NO_3^-/NO_2^- and NH_4^+.[64] Consistently, light-off experiments of the monolithic bifunctional catalyst system performed at water vapor concentrations representative of real hydrogen internal combustion engine exhaust (0–20 vol% H_2O)[65] reveal only a minor effect of increasing humidity levels on catalyst performance (*cf.* Fig. S8) and thus underscore the potential of the bifunctional catalyst proposed herein for efficient deNO_x in H_2-ICE applications (Fig. 9).

Conclusions

This study systematically evaluated Pd-based catalysts for H_2-SCR of NO_x under conditions representative of H_2-ICE exhaust. The key aspects identified in this work to govern catalyst performance are summarized in schematic Fig. 9. Catalysts supported on TiO_2-modified HY zeolite showed that decreasing Pd loading raised NO and H_2 light-off temperatures, indicating diminished low-temperature activity. Kinetic analysis indicates that NO conversion at low temperatures is limited by H_2 activation, whereas competitive H_2 oxidation dominates at higher temperatures, hereby hampering NO reduction. Water vapor suppressed NO conversion across all formulations. Pd dispersion strongly influenced product selectivity: lower Pd

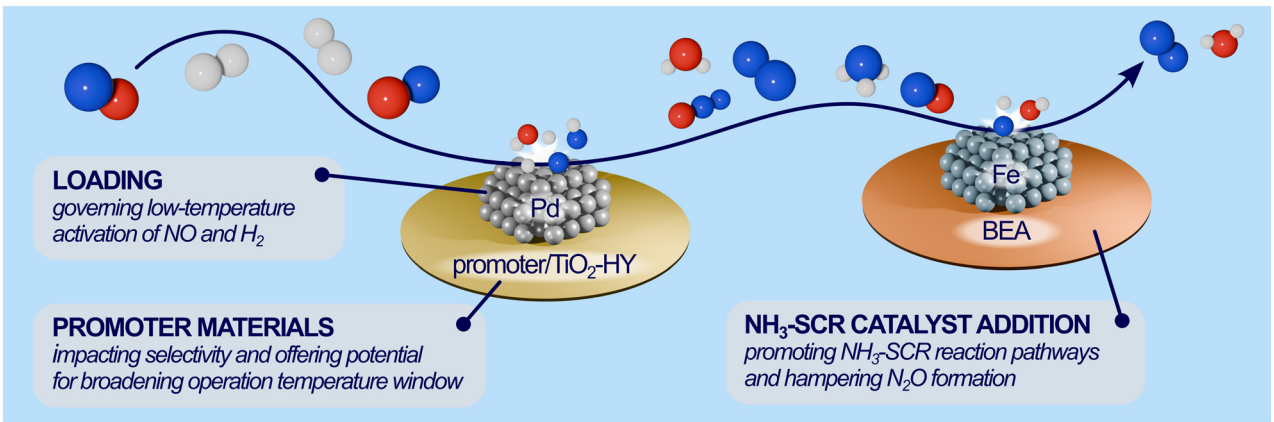

Fig. 9 Illustrative summary of key factors driving catalyst performance and their mechanistic implications.

loadings promoted NH_3 formation above 200 °C, while N_2O remained a persistent byproduct regardless of the noble metal loading. Variations in surface area may also affect performance, likely through changes in surface site density of acidic sites. While all HY-supported catalysts were synthesized *via* simple TiO_2 precipitation and Pd impregnation for the present study, the results suggest that more advanced synthesis methods are needed in the future to better control support morphology and metal particle size for clearer structure–activity correlations.

Composite catalysts were also explored to broaden the effective temperature window. Adding V_2O_5 improved N_2 selectivity but reduced NO conversion, particularly under humid conditions. In contrast, WO_3 incorporation enhanced low-temperature (100–175 °C) NO conversion and minimized NH_3 formation, though N_2O production above 200 °C remained problematic.

To mitigate byproduct formation more efficiently, a bifunctional system combining Pd/TiO_2/HY with Fe-BEA was developed. This composite catalyst improved NO conversion under both dry and humid conditions and significantly reduced NH_3 and N_2O formation, achieving >90% N_2 selectivity between 180 and 300 °C in realistic humid conditions (powder catalyst testing). Monolith testing confirmed stable performance over 12 hours. Spatially resolved measurements showed NH_3 formation near the inlet, attributable to BEA Brønsted acid sites, and downstream consumption *via* Fe-mediated NH_3-SCR pathways, collectively contributing to lower N_2O formation. The relative contributions of these pathways to the overall performance, however, require further clarification.

Future work should employ *operando* spectroscopic methods to – preferentially simultaneously – elucidate electronic and mechanistic features governing bifunctional catalyst behavior. The strong synergies observed in the Pd/TiO_2-HY + Fe-BEA system highlight its promise for advancing H_2-SCR toward practical H_2-ICE emission control applications.

Author contributions

Michael Borchers: conceptualization, data curation, formal analysis, investigation, validation, visualization, writing – original draft. Daniel Hodonj: data curation, formal analysis, investigation, methodology, validation, visualization, writing – original draft. Kathrin Schäfer: formal analysis, investigation. Frank Manuel Bauer: formal analysis, investigation. Patrick Lott: conceptualization, data curation, funding acquisition, methodology, project administration, resources, supervision, validation, visualization, writing – original draft.

Conflicts of interest

There are no conflicts to declare.

Data availability

The data supporting this article have been included as part of the supplementary information (SI).

Supplementary information is available. See DOI: https://doi.org/10.1039/d5cy01387a.

Acknowledgements

The authors acknowledge O. Deutschmann for fruitful discussion and support regrading resources, S. Kurukunda for the N_2-physisorption measurements, A. De Giacinto for the XRD measurements (all ITCP, KIT), and T. Bergfeldt (IAM-AWP, KIT) for the ICP-OES-measurements. Financial support by the German Federal Ministry for Economic Affairs and Energy through project PoWer (FKZ 19I24003F) and by the Helmholtz program "Materials and Technologies for the Energy Transition" (MTET) is gratefully acknowledged. Also, this work was funded by the Deutsche Forschungsgemeinschaft (DFG, German Research Foundation) – SFB 1441 – Project-ID 426888090.

References

1 P. Lott, U. Wagner, T. Koch and O. Deutschmann, *Chem. Ing. Tech.*, 2022, **94**, 217–229.
2 Y. H. Teoh, H. G. How, T. D. Le, H. T. Nguyen, D. L. Loo, T. Rashid and F. Sher, *Fuel*, 2023, **333**, 126525.
3 Z. Hu and R. T. Yang, *Ind. Eng. Chem. Res.*, 2019, **58**, 10140–10153.
4 S. Muhammad Farhan, W. Pan, C. Zhijian and Y. JianJun, *Fuel*, 2024, **355**, 129364.
5 M. N. Khan, D. Peng, S. Hu, X. Wang, X. Lin, L. Han, Z. Hu, J. Zou and D. Zhang, *Int. J. Hydrogen Energy*, 2025, **151**, 150183.
6 M. Jabłońska and A. Osorio Hernández, *ChemCatChem*, 2024, **16**, e202400977.
7 K. Polychronopoulou and A. M. Efstathiou, *Recent Pat. Mater. Sci.*, 2012, **5**, 87–104.
8 C. Yin, L. Wang, S. Rivillon, A. J. Shih and R. T. Yang, *Catal. Lett.*, 2015, **145**, 1491–1499.
9 J. Shao, P. H. Ho, D. Creaser and L. Olsson, *Appl. Catal. O: Open*, 2024, **188**, 206947.
10 P. Granger, F. Dhainaut, S. Pietrzik, P. Malfoy, A. S. Mamede, L. Leclercq and G. Leclercq, *Top. Catal.*, 2006, **39**, 65–76.
11 M. Mihet, M. D. Lazar, V. Almasan and V. Mirel, *AIP Conf. Proc.*, 2012, **1425**, 73–76.
12 X. Li, X. Zhang, Y. Xu, Y. Liu and X. Wang, *Chin. J. Catal.*, 2015, **36**, 197–203.
13 Z. Savva, K. C. Petallidou, C. M. Damaskinos, G. G. Olympiou, V. N. Stathopoulos and A. M. Efstathiou, *Appl. Catal., A*, 2021, **615**, 118062.
14 M. Jabłońska, A. Osorio Hernández, J. Dornseiffer, J. Grams, A. Guo, U. Simon and R. Gläser, *Catalysts*, 2025, **15**, 483.
15 S. Xu, Z. Liu, C. Peng and Z. Liu, *ACS Appl. Nano Mater.*, 2025, **8**, 4760–4769.
16 M. Machida, S. Ikeda, D. Kurogi and T. Kijima, *Appl. Catal., B*, 2001, **35**, 107–116.
17 G. Jong Kim, J. Hun Shin, S. Bin Kim and S. Chang Hong, *Appl. Surf. Sci.*, 2023, **608**, 155040.
18 S. Xu, R. Li, J. Chen and Z. Liu, *ACS Appl. Nano Mater.*, 2023, **6**, 9322–9330.
19 Q. Yu, M. Richter, L. Li, F. Kong, G. Wu and N. Guan, *Catal. Commun.*, 2010, **11**, 955–959.

20 X. Zhang, X. Wang, X. Zhao, Y. Xu, H. Gao and F. Zhang, *Chem. Eng. J.*, 2014, **252**, 288–297.
21 X. Zhang, X. Wang, X. Zhao, Y. Xu, Y. Liu and Q. Yu, *Chem. Eng. J.*, 2015, **260**, 419–426.
22 X. Zhao, X. Zhang, Y. Xu, Y. Liu, X. Wang and Q. Yu, *J. Mol. Catal. A: Chem.*, 2015, **400**, 147–153.
23 L. Cao, Q. Wang and J. Yang, *J. Environ. Chem. Eng.*, 2020, **8**, 103631.
24 S. Xie, L. Liu, Y. Li, K. Ye, D. Kim, X. Zhang, H. Xin, L. Ma, S. N. Ehrlich and F. Liu, *Nat. Commun.*, 2024, **15**, 7988.
25 M. Machida and T. Watanabe, *Appl. Catal., B*, 2004, **52**, 281–286.
26 L. Li, F. Zhang, N. Guan, E. Schreier and M. Richter, *Catal. Commun.*, 2008, **9**, 1827–1832.
27 Y. Zhang, S. Xu, J. Li, E. He and Z. Liu, *J. Phys. Chem. C*, 2023, **127**, 7248–7256.
28 S. Cimino, E. M. Cepollaro, M. E. Fortunato and L. Lisi, *Catalysts*, 2025, **15**, 598.
29 M. Leicht, F. J. P. Schott, M. Bruns and S. Kureti, *Appl. Catal., B*, 2012, **117–118**, 275–282.
30 E. Eßer, D. Schröder, A. V. Nartova, A. M. Dmitrachkov and S. Kureti, *Catal. Lett.*, 2022, **152**, 1598–1610.
31 E. Eßer, D. Schröder and S. Kureti, *J. Catal.*, 2023, **423**, 129–144.
32 N. Macleod and R. M. Lambert, *Catal. Lett.*, 2003, **90**, 111–115.
33 G. Qi, R. T. Yang and F. C. Rinaldi, *J. Catal.*, 2006, **237**, 381–392.
34 L. Warmuth, P. Lott, O. Deutschmann and C. Feldmann, *ChemCatChem*, 2023, **15**, e202201354.
35 J. Shibata, M. Hashimoto, K.-i. Shimizu, H. Yoshida, T. Hattori and A. Satsuma, *J. Phys. Chem. B*, 2004, **108**, 18327–18335.
36 M. Borchers, P. Lott and O. Deutschmann, *Top. Catal.*, 2023, **66**, 973–984.
37 P. Chen, M. Jabłońska, P. Weide, T. Caumanns, T. Weirich, M. Muhler, R. Moos, R. Palkovits and U. Simon, *ACS Catal.*, 2016, **6**, 7696–7700.
38 S. Brunauer, P. H. Emmett and E. Teller, *J. Am. Chem. Soc.*, 1938, **60**, 309–319.
39 J. Schütz, H. Störmer, P. Lott and O. Deutschmann, *Catalysts*, 2021, **11**, 300.
40 G. Bergeret and P. Gallezot, in *Handbook of Heterogeneous Catalysis*, 2008, pp. 738–765, DOI: 10.1002/9783527610044.hetcat0038.
41 M. Borchers, K. Keller, P. Lott and O. Deutschmann, *Ind. Eng. Chem. Res.*, 2021, **60**, 6613–6626.
42 K. Keller, D. Hodonj, L. Zeh, L. Caulfield, E. Sauter, C. Wöll, O. Deutschmann and P. Lott, *Catal. Sci. Technol.*, 2024, **14**, 4142–4153.
43 T. Hlavatý, P. Kočí, M. Isoz, D. Deka and W. Partridge, *Chem. Eng. Sci.*, 2023, **282**, 119272.
44 J. H. Holles, R. J. Davis, T. M. Murray and J. M. Howe, *J. Catal.*, 2000, **195**, 193–206.
45 M. Benkhaled, S. Morin, C. Pichon, C. Thomazeau, C. Verdon and D. Uzio, *Appl. Catal., A*, 2006, **312**, 1–11.
46 Z. Zhang, J. Lu, B. Zhang, W. Shi, Y. Guo and F. Cui, *Environ. Sci.: Nano*, 2020, **7**, 2117–2129.
47 T. J. Eldridge, M. Borchers, P. Lott, J.-D. Grunwaldt and D. E. Doronkin, *Catal. Sci. Technol.*, 2024, **14**, 4198–4210.
48 A. Ueda, T. Nakao, M. Azuma and T. Kobayashi, *Catal. Today*, 1998, **45**, 135–138.
49 Z. Liu, Y. Lu, L. Yuan, L. Ma, L. Zheng, J. Zhang and T. Hu, *Appl. Catal., B*, 2016, **188**, 189–197.
50 K. Duan, Z. Liu, J. Li, L. Yuan, H. Hu and S. I. Woo, *Catal. Commun.*, 2014, **57**, 19–22.
51 O. Feeley and W. Sachtler, *Appl. Catal.*, 1990, **67**, 141–150.
52 B. Bromley, C. Pischetola, L. Nikoshvili, F. Cárdenas-Lizana and L. Kiwi-Minsker, *Molecules*, 2020, **25**, 3867.
53 M. L. Bols, B. E. R. Snyder, H. M. Rhoda, P. Cnudde, G. Fayad, R. A. Schoonheydt, V. Van Speybroeck, E. I. Solomon and B. F. Sels, *Nat. Catal.*, 2021, **4**, 332–340.
54 P. Boroń, L. Chmielarz, J. Gurgul, K. Łątka, T. Shishido, J.-M. Krafft and S. Dzwigaj, *Appl. Catal., B*, 2013, **138–139**, 434–445.
55 J. Zeng, S. Chen, Z. Fan, C. Wang, H. Chang and J. Li, *Ind. Eng. Chem. Res.*, 2020, **59**, 19500–19509.
56 J. A. Z. Pieterse, G. D. Pirngruber, J. A. van Bokhoven and S. Booneveld, in *Studies in Surface Science and Catalysis*, ed. R. Xu, Z. Gao, J. Chen and W. Yan, Elsevier, 2007, vol. 170, pp. 1386–1391.
57 A. Grossale, I. Nova, E. Tronconi, D. Chatterjee and M. Weibel, *J. Catal.*, 2008, **256**, 312–322.
58 H. Y. Huang, R. Q. Long and R. T. Yang, *Appl. Catal., A*, 2002, **235**, 241–251.
59 R. Q. Long and R. T. Yang, *J. Catal.*, 2002, **207**, 224–231.
60 A. Guzmán-Vargas, G. Delahay and B. Coq, *Appl. Catal., B*, 2003, **42**, 369–379.
61 Q. Liu, C. Bian, S. Ming, L. Guo, S. Zhang, L. Pang, P. Liu, Z. Chen and T. Li, *Appl. Catal., A*, 2020, **607**, 117865.
62 D. Klukowski, P. Balle, B. Geiger, S. Wagloehner, S. Kureti, B. Kimmerle, A. Baiker and J.-D. Grunwaldt, *Appl. Catal., B*, 2009, **93**, 185–193.
63 Y. Dong, T. Zhang, Y. Zhang, J. Du, Y. Sun, Z. Liu, W. Ding, Y. Shan, W. Shan and H. He, *Applied Catalysis B: Environment and Energy*, 2025, **371**, 125217.
64 J. Shi, Y. Zhang, Z. Zhang, Z. Fan, M. Chen, Z. Zhang and W. Shangguan, *Catal. Commun.*, 2018, **115**, 59–63.
65 Y. Chen, D. Lou, Y. Zhang, L. Fang, D. Yang, D. Ren and G. Song, *Int. J. Hydrogen Energy*, 2024, **81**, 1181–1191.